HHS Public Access

Author manuscript

Toxicology. Author manuscript; available in PMC 2021 December 01.

Published in final edited form as:

Toxicology. 2020 December 01; 445: 152601. doi:10.1016/j.tox.2020.152601.

Human *In Vitro* Vascularized Micro-Organ and Micro-Tumor Models are Reproducible Organ-on-a-Chip Platforms for Studies of Anticancer Drugs

Yizhong Liu[1,2], **Courtney Sakolish**[1,2], **Zunwei Chen**[1,2], **Duc T.T. Phan**[3], **R. Hugh F. Bender**[3], **Christopher C.W. Hughes**[3,4], **Ivan Rusyn**[1,2,‡]

[1]Interdisciplinary Faculty of Toxicology, Texas A&M University, College Station, TX, 77843, USA

[2]Department of Veterinary Integrative Biosciences, Texas A&M University, College Station, TX, 77843, USA

[3]Department of Molecular Biology and Biochemistry, University of California, Irvine, Irvine, CA, 92697, USA

[4]Department of Biomedical Engineering, University of California, Irvine, Irvine, CA, 92697, USA

Abstract

Angiogenesis is a complex process that is required for development and tissue regeneration and it may be affected by many pathological conditions. Chemicals and drugs can impact formation and maintenance of the vascular networks; these effects may be both desirable (e.g., anti-cancer drugs) or unwanted (e.g., side effects of drugs). A number of *in vivo* and *in vitro* models exist for studies of angiogenesis and endothelial cell function, including organ-on-a-chip microphysiological systems. An arrayed organ-on-a-chip platform on a 96-well plate footprint that incorporates perfused microvessels, with and without tumors, was recently developed and it was shown that survival of the surrounding tissue was dependent on delivery of nutrients through the vessels. Here we describe a technology transfer of this complex microphysiological model between laboratories and demonstrate that reproducibility and robustness of these tissue chip-enabled experiments depend primarily on the source of the endothelial cells. The model was highly reproducible between laboratories and was used to demonstrate the advantages of the perfusable vascular networks for drug safety evaluation. As a proof-of-concept, we tested Fluorouracil (1–1,000 μM), Vincristine (1–1,000 nM), and Sorafenib (0.1–100 μM), in the perfusable and non-perfusable

‡To whom correspondence should be addressed: Ivan Rusyn, MD, PhD, Department of Veterinary Integrative Biosciences, Texas A&M University, College Station, TX 77843; irusyn@cvm.tamu.edu; (979) 458-9866.

Conflict of Interest Statement: C.C.W.H. is a founder and major shareholder of Aracari Biosciences, which is commercializing some of the technology described in this manuscript. D.T.T.P. and R.H.F.B. serve as scientists at Aracari Biosciences and receive stock and financial compensation from Aracari Biosciences. The terms of these arrangements have been reviewed and approved by the University of California, Irvine in accordance with its conflict of interest policies.

Declaration of interests

The authors declare that they have no known competing financial interests or personal relationships that could have appeared to influence the work reported in this paper.

micro-organs, and in a colon cancer-containing micro-tumor model. Tissue chip experiments were compared to the traditional monolayer cultures of endothelial or tumor cells. These studies showed that human *in vitro* vascularized micro-organ and micro-tumor models are reproducible organ-on-a-chip platforms for studies of anticancer drugs. The data from the 3D models confirmed advantages of the physiological environment as compared to 2D cell cultures. We demonstrated how these models can be translated into practice by verifying that the endothelial cell source and passage are critical elements for establishing a perfusable model.

Keywords

Endothelial cell; microphysiological system; drug safety evaluation; tissue chip

1. Introduction

The vascular system can be impacted by a wide variety of intrinsic and extrinsic factors that include congenital and diet-associated diseases (Ross et al. 2018; Zito et al. 2020), drugs (Pinheiro et al. 2020), and environmental factors (Lawal et al. 2016). Endothelial cells (EC) play a critical role in maintaining integrity of the vascular system, providing the structural foundation of blood vessels and contributing to the regulation of vascular tone (Peng et al. 2019). Most of the information on the role that EC play in health and disease comes from whole animal or clinical studies (Semeraro et al. 2015), or *in vitro* studies of EC in culture (Grimm et al. 2020; Iwata et al. 2017; Nowak-Sliwinska et al. 2018). The *in vitro* studies are typically restricted to assays of EC viability, proliferation, and/or migration such as tube formation (Hadzijusufovic et al. 2017; Iruela-Arispe and Davis 2009; Nakatsu et al. 2003; Nguyen et al. 2017). More complex human vascular microphysiological systems (MPS) represent promising 3D *in vitro* models of normal (Jeon et al. 2015; Moya et al. 2013; Nguyen et al. 2013; Phan et al. 2017; Sobrino et al. 2016; Yeon et al. 2012) and diseased (Atchison et al. 2017) vascular tissue; a number of such models have been recently developed (Zhang et al. 2020).

Two functions of the vasculature system are of particular interest in drug efficacy and safety studies – angiogenesis and blood vessel permeability. Tumor growth and metastasis require formation of blood vessels within the tumor area (Barillari 2020) where new vessels may originate from outgrowth of pre-existing vessels (angiogenesis) and/or the differentiation of bone marrow-derived stem cells that differentiate into mature EC (vasculogenesis). Inhibition of tumor re-vascularization is a common modality for cancer chemotherapeutics, and a number of kinase inhibitors have been developed that block angiogenesis (Viallard and Larrivee 2017). *In vitro* studies in EC have been also used to demonstrate drug-specific toxicity and impaired angiogenesis with a number of atherosclerosis-associated drugs (Hadzijusufovic et al. 2017). At the same time, hemorrhage is a common side effect of many cancer drugs, an effect that is thought to be associated with disruption of vascular endothelial growth factor (VEGF)-mediated signaling pathways (Lacal and Graziani 2018). To investigate the potential liability of hemorrhage, as well as to differentiate the effects of drugs on the tumor as opposed to the vasculature *in vitro*, a perfusable vascular network must be established, which is achievable only using MPS. The microfluidic devices that

comprise a vascularized micro-organ or micro-tumor have been established using extracellular matrix-embedded co-culture of endothelial and tumor cells in a microfluidic device (Hachey and Hughes 2018; Moya et al. 2013). These studies showed that growth of the tumor clusters and delivery of the drugs to the tumor were enabled by flow through the vascular network (Phan et al. 2017; Sobrino et al. 2016). This MPS has been scaled to multi-well plate format to improve both throughput and relevance (Phan et al. 2017; Sobrino et al. 2016). Real-time study of drug responses and tumor-stromal interactions in this novel three-dimensional model showed that gene expression, tumor characteristics and drug responses reflect closely clinical observations in colorectal cancer, as compared to standard monolayer cultures or spheroids (Hachey et al. 2020).

While there are many promising findings in MPS that have been reported by the laboratories that develop tissue chips, the wide-spread use and application of MPS to drug and chemical safety studies is often limited because of the technical challenges, availability of the devices or cells, and lack of independent replication of the findings (Ewart et al. 2017; Livingston et al. 2016; Marx et al. 2020). Several recent studies showed that complex MPS can be successfully transferred between laboratories (Maass et al. 2019; Sakolish et al. 2020; Sakolish et al. 2018). These studies not only provide evidence of the robustness of the complex models, but also facilitate translation of MPS to practice. Accordingly, the present study focused on establishing the reproducibility and robustness of a human vascularized micro-tumor model (Hachey et al. 2020; Phan et al. 2017). We successfully demonstrated technology transfer, established the importance of the cell source for formation of the functional model, confirmed reproducibility of the model across EC sources, and confirmed the advantage of the MPS as compared to monolayer cultures with respect to drug effects.

2. Materials and Methods

2.1. Microfluidic microphysiological system.

Microfluidic devices (Figure 1A) used in this study were fabricated at the Hughes lab (Department of Molecular Biology and Biochemistry) at the University of California, Irvine as previously described (Phan et al. 2017; Sobrino et al. 2016). Specifically, polydimethylsiloxane (PDMS, Ellsworth Adhesives, Germantown, WI) was poured into a customized polyurethane master mold and allowed to polymerize overnight in a 70°C oven. The PDMS replicate layer was removed and holes were punched to create inlets and outlets for the media reservoirs and loading chambers. The PDMS device was attached to a 96-well open-bottom plastic culture plate via chemical gluing and oxygen plasma bonding using a plasma cleaner (Harrick Plasma, Ithaca, NY), after which a transparent 150 μm PDMS membrane was then bonded to the device using oxygenated plasma. The fully assembled device was placed in a 60°C oven overnight, covered with a standard 96-well plate polystyrene lid, and sterilized with UV light for 30 minutes prior to use. A total of 12 or 16 microfluidic device units were bonded to a bottomless 96-well plate; a single device unit contains 3 connected tissue chambers that are fed through microfluidic channels. Cells (EC, fibroblasts and cancer cells) and extracellular matrix are injected into the tissue chambers using a pipette as detailed elsewhere (Phan et al. 2017) and media is perfused through microfluidic channels using gravity-driven flow.

2.2. Cells.

Samples of de-identified human primary endothelial progenitor cells (EPC) and primary human umbilical vein endothelial cells (HUVEC) were obtained from the Hughes Lab (University of California-Irvine). Five EPC lines (EPC-N, EPC-AD, EPC-D8, EPC-10, EPC-BG) and 2 HUVEC lines (HUVEC-216, HUVEC 155) were tested in this study. These cells were isolated from cord blood or umbilical cords with IRB approval, selected for the CD31+ cell population, and expanded on gelatin-coated flasks in EGM-2 medium (CC-3162; Lonza, Walkersville, MD). All cells were used between passages 5–8. Normal human lung fibroblasts (NHLFs, CC-2515) were obtained from Lonza. Colorectal cancer cell line (HCT116) were donated from the UC Irvine Chao Family Comprehensive Cancer Center. Both NHLF and HCT116 cells were cultured in Dulbecco's modified Eagle's medium (DMEM, 10-013-CV; Corning, Corning, NY) supplemented with 10% fetal bovine serum (FBS, 97068–091; VWR, Radnor, PA) and 5 μg/mL gentamicin (15710064; Gibco, Waltham, MA). Endothelial and HCT116 cells were transduced with lentivirus expressing mCherry (LeGO-C2, plasmid #27339; Addgene, Cambridge, MA) or Azurite (pLV-Azurite, plasmid #36086; Addgene).

2.3. Device loading and cell culture in MPS.

Device loading followed previously reported protocols (Phan et al. 2017; Sobrino et al. 2016) with minor modifications. Specifically, a concentration of 10 mg/mL fibrinogen solution was prepared by gently dissolving 70% clottable bovine fibrinogen (F8630; Sigma-Aldrich, St. Louis, MO) in 1× phosphate buffered saline (PBS; Sigma-Aldrich), then filtered through a 0.2 μm filter. The final matrix solution for cell suspension consisted of 80% of the 10 mg/mL fibrinogen solution and 20% of 1 mg/mL human fibronectin (356008, Corning). For vascularized micro-organ (VMO) experiments, EC and NHLFs were resuspended in the matrix solution to a final concentration of 10 or 7 million cells/mL, respectively. For vascularized micro-tumor (VMT) experiments, HCT116 cells were added to the endothelial and NHLF cell suspension at 100,000 cells/mL. Prior to device loading, 5 μL of the final cell-matrix suspension was mixed with 2 μL of 50 U/mL thrombin (T4648; Sigma-Aldrich) to initiate polymerization, then quickly injected into the device through the gel loading inlet. After loading, devices were incubated at 37°C for 15 minutes. Next, the microfluidic channels were coated with 1 mg/mL laminin (23017015; Fisher Scientific, Waltham, MA) by injecting 5 μL of 1 mg/mL laminin through the media perfusion channels, followed by an additional 10-minute incubation at 37 °C. EGM-2 cell culture medium was then introduced into the system and a 5-mm H_2O interstitial pressure across the tissue chambers was established by adding 350 μL and 50 μL EGM-2 to the upstream and downstream medium reservoirs, respectively. Medium in the reservoirs was changed every day to maintain the interstitial flow. All devices were imaged daily using a temperature- and CO_2-controlled confocal imaging system (ImageXpress Micro Confocal High Content Imaging System; Molecular Devices, San Jose, CA). Anastomosis of the endothelial microvascular network was confirmed by perfusing the devices with 70 kDa FITC-Dextran (FD70S; Sigma-Aldrich) through the network on day 6 post-loading under the confocal imaging system.

2.4. Cell culture in monolayers.

EC and HCT116 colorectal cancer cells were seeded in separate 96-well plates at a seeding density of 5,000 cells/well in 100 μL of their respective media (see above) and incubated for 24 hours prior to drug exposure. Cells were then exposed to treatments at the same concentrations as in MPS devices for 48 hours. Cell viability was quantified using CellTiter-Glo® Luminescent Cell Viability Assay (G7573; Promega, Madison, WI) following the manufacturer's instructions. Briefly, a volume of CellTiter-Glo reagent solution equal to the volume of cell culture medium present in each well was added to each well in the 96-well plate after the plate and its contents were equilibrated to room temperature, mixed on an orbital shaker for 2 minutes to induce cell lysis, and incubated at room temperature for 10 minutes to allow stabilized luminescent signal. Luminescence was read using FLIPR Tetra High-Throughput Cellular Screening System (Molecular Devices). For each dose, viability values were averaged across technical replicates and then normalized to vehicle.

2.5. Drug treatments.

To demonstrate the application of the vascularized MPS for studies of drug effects, microfluidic devices and 2D cell cultures of endothelial and tumor cells were exposed to three test compounds. FDA-approved anti-cancer drugs Fluorouracil (5-FU, S1209; concentrations tested: 1, 10, 100, 300, 1000 μM), Vincristine (S1241; concentrations tested: 1, 10, 100, 300, 1000 nM), and Sorafenib (S7397; concentrations tested: 0.1, 1, 10, 30, 100 μM), were purchased from Selleckchem (Houston, TX). All test compounds were dissolved in 100% cell culture grade dimethyl sulfate (DMSO, Fisher Scientific) to 200 mM for 5-FU and Vincristine and 20 mM for Sorafenib (i.e., 200× of the top test concentration). Final concentration of DMSO vehicle was 0.5% v/v in all conditions. Drug or vehicle treatments were introduced to the microfluidic devices through cell culture medium channels and reservoirs on day 6 post-loading. The interstitial flow was maintained by transferring cell culture medium from the outlet reservoir to the inlet reservoir daily to re-establish the interstitial pressure. Cell culture medium with drugs and/or vehicle was replaced with fresh EGM-2 on day 8 and the devices were monitored for another 2 days until day 10.

2.6. Vascular permeability quantification.

For vascular permeability measurements, an imaging-based fluorescent intensity analysis was used to quantify the permeability of the microvascular vessel network. On day 6 post-loading, the medium in the microfluidic device was replaced by EGM-2 containing 50 μg/mL of 70kDa FITC-Dextran with the same hydrostatic pressure profile as before. A fluorescent image of the background was taken prior to the addition of FITC-Dextran. After the dye perfused into the vascular network (approximately 15 minutes after initiating the interstitial flow), an initial fluorescent image was taken (*t0*). Another fluorescent image was taken at the end of the 90-minute perfusion (*t90*). The permeability coefficient P was then calculated using the following equation as described previously (Jeon et al. 2014):

$$P = \frac{1}{I_0 - I_b}\left(\frac{I_{90} - I_0}{\Delta t}\right) \times \frac{D}{4}$$

where I_0, I_{90}, and I_b represent the fluorescent intensity of the images taken at t_0, t_{90}, and before the addition of FITC-Dextran, respectively, Δt is the time interval between t_0 and t_{90}, and D is the average diameter of the vessel.

2.7. Tumor growth quantification and microvascular vessel network characterization in 3D microfluidic devices.

To quantify tumor growth, progression, and endothelial vessel network development in the 3D microfluidic devices, the devices were imaged using ImageXpress Micro Confocal High Content Imaging System (Molecular Devices). For tumor growth quantification, fluorescent intensity and area of fluorescent HCT116 cells images was measured using ImageJ software (National Institutes of Health), and tumor growth was quantified as the value of intensity multiplied by the area. For microvascular vessel network characterization, fluorescent images of the vasculature were analyzed using AngioTool software (National Institute of Health) to derive total vessel length, average vessel length, vessel area, and total number of junctions. Vessel diameter was quantified using ImageJ by measuring the cross-distance perpendicular to the vessel wall. For each device, multiple non-overlapping measurements were taken and data were averaged.

2.8. Statistical analysis.

All analyses were performed with Excel (Microsoft Office Professional Plus 2016, Microsoft, Redmond, WA) or GraphPad Prism 7 (GraphPad Software Inc., La Jolla, CA). Data were analyzed using one-way ANOVA followed by post hoc Dunnett's test, or two-way ANOVA followed by either Sidak or Tukey post hoc tests. All presented data are mean ± standard error of the mean (SEM), p values <0.05 were considered significant.

2.9 Timeline to establish devices.

Once molds have been fabricated, device construction takes about one day (and multiple plates can be made at once). Cell preparation and loading takes about 2–3 hours for a single, 16-device plate. Vascular networks form in 3–5 days, depending on the cell lines used.

3. Results and Discussion

3.1. Technology transfer of the vascularized micro-organ and -tumor models.

As the first step of adopting a new MPS into basic research and pre-clinical drug evaluation, the functionality and reliability need to be established through technology transfer from the developers to end-users (Sakolish et al. 2018). MPS are inherently more complex than traditional cell culture because of the need for the specialized microfluidic devices and special skills to seed and culture cells in these devices under media flow. As the first step in the experiments detailed in this manuscript, research staff from TEX-VAL Tissue Chip Testing (Laboratory 1) were trained in Dr. Hughes' laboratory (Laboratory 2) at the Department of Molecular Biology and Biochemistry at the University of California, Irvine. Hands-on practice in handling the devices and detailed protocols were part of technology transfer. For the future users of this technology, all data and protocols reported in this manuscript are available (see the links in Supplemental Table 1) through the Microphysiology Systems Database (Schurdak et al. 2020).

Primary EC (EPC-N at passage 5) and fibroblasts (NHLFs) were mixed with gel matrix and loaded into devices (Figure 1A) as detailed in Methods (section 2.3). Devices were maintained under gravimetric flow; as demonstrated previously (Phan et al. 2017), successfully loaded device units developed robust and uniform vascular networks over about 1-week post-loading in both laboratories (Figures 1B–C). Presence of perfusable vessels in the networks was confirmed by introducing FITC-Dextran (70 kDa) into one of the microfluidic channels and observing vascular network-directed flow of the fluorescence substance through the vessels that were formed. Equally successful experiments were performed in Laboratory 1 (Figure 1B) and Laboratory 2 (Figure 1C) demonstrating successful technology transfer of the complex MPS from the developers to end-users.

We compared performance of the vascularized micro-organs (EC and fibroblasts) to vascularized micro-tumors (EC, fibroblasts and HCT116 colon cancer cells). Figures 2A–B show representative tissue chambers for devices without and with HCT116 cells. In vascularized micro-tumors (Figure 2B), cancer cells formed foci that were often attached to the vascular network. Previous studies (Hachey et al. 2020) conducted comparisons between vessels in the presence or absence of tumor cells and demonstrated vessel irregularity and compression becoming more pronounced at later time points, especially as the tumors grow larger by day 8 of culture. This study found that the vasculature within the vascularized micro-tumors was leakier and the total vessel length, diameter and the number of junctions were lower than in the non-tumor containing devices. In our experiments, a time-course FITC-Dextran perfusion experiment was performed on both types of devices; however, we found no difference between vascularized micro-organs and micro-tumors on a number of quantitative phenotypes pertaining to the vasculature network and its permeability (Figure 2C). The experiments reported herein and those reported by Hachley et al. (2020) differed in the time point when the measurements were taken (day 8 vs day 6, respectively) and this is likely the primary reason of the discordant findings. Still, we examined and compared the variability among the devices in the same experiment as another metric of reproducibility. It was shown that the total vessel length and vessel area were highly consistent among different experiments in vascularized micro-organs, and similar to those observed in 2D monolayer cultures (Phan et al. 2017). In our experiments in vascularized micro-organs, nearly identical coefficient of variability (CV) values of 12–13% were observed; however, much greater variability (17–18% CV) was found in vascularized micro-tumors. For other phenotypes describing the vascular network's organization, such as average vessel length, number of junctions, vessel diameter, the CVs were 20–35% in both types of devices, the variability in tumor cell-containing devices was almost always greater than that in vascularized micro-organs. Vessel permeability was the most variable phenotype, with CV of 55% in vascularized micro-organ and 92% in vascularized micro-tumors. Structural heterogeneity of tumor-associated vasculature was studied in detail by Hachley et al. (2020) who showed that vascularized micro-tumors contain both highly leaky areas and those that are ill- or non-perfused. Thus, the findings of greater heterogeneity in tumor cell-containing devices observed in both studies are consistent with previous reports that *de novo* formed tumor vasculature networks are highly irregular (Yu et al. 2001), likely as a result of disrupted microenvironment cues (Carmeliet and Jain 2011).

3.2. The role of cell source in performance of the vascularized micro-organ and -tumor models.

Another potential reason for the difference in the vascular networks observed in the studies in different laboratories is the use of different EC. Indeed, the importance of cell source in reproducibility of studies in MPS has been recently shown (Sakolish et al. 2018). Thus, study-to-study variability introduced by the cell source is an important potential source of discordance among publications and needs to be characterized also in relationship to the MPS. Both hemodynamic and molecular forces contribute to the formation of new vascular lumens during blood vessel morphogenesis (Gebala et al. 2016). Because microfluidic devices used in these studies are near identical in the media flow conditions, we studied the ability of different EC preparations to form perfusable networks in vascularized micro-organs (Figure 3). In research on EC, vasculogenesis has been a primary focus as it reflects the ability of EC to develop and form blood vessels (Jain et al. 1998; Lamalice et al. 2007; Norton and Popel 2016). However, most in vitro models are only able to confirm and quantify the development of the vessel network two-dimensionally, whether such networks are lumenized remains unknown (Craige et al. 2011; Iwata et al. 2017; Kaur et al. 2010). To test the capacity for lumenization of different EC, seven preparations of primary EC lines (EPC-N, EPC-AD, EPC-D8, EPC-10, EPC-BG, HUVEC-155, and HUVEC-216) were loaded into the devices with supporting NHLFs, monitored daily under a confocal imaging system, and FITC-Dextran perfusion was performed on day 6 post-loading (Figure 3). All EC lines were received by our laboratory at passage 4 to 6 and were used to construct vascularized micro-organs after only one or two additional passages to expand the cell numbers to sufficient quantities for experiments. Even though all seven cell lines formed vascular networks by day 6 in culture, only three lines formed the networks with a lumen that could be perfused with FITC-Dextran.

EC used in *in vitro* studies of vasculogenesis are not immortalized and undergo a finite number of cell divisions before growth arrest or replicative senescence (Dewberry et al. 2003; Erusalimsky 2009). In turn, EC senescence in tissue culture has been associated with EC dysfunction and impaired capacity for vasculogenesis (Celermajer et al. 1994; Rivard et al. 1999; van der Loo et al. 2000; Weinsaft and Edelberg 2001). To further investigate cell passage-dependent ability of the EC to form perfusable networks, we tested EPC-N cells at passage 5 and passage 8 (Figure 3). While cells at passage 5 formed well-perfusable vascular networks, vasculogenesis was impaired and no lumen formed with cells at passage 8. These results indicate that not all EC preparations can form perfusable vessel networks even if the vessel network is developed, and that the angiogenesis and lumenization of EC are greatly dependent on the age of cells in culture. The latter observation is most important for the use of this MPS in future experiments as a different source of cells, such as those derived from induced pluripotent stem cells (iPSC), may be needed to address donor-to-donor variability that is currently inherent in the *in vitro* studies of EC.

A comparison of vascularized micro-tumors was also performed where the principal variable was the type of the EC used (Figure 4). In these experiments, we used three primary EC lines that were able to develop perfusable microvascular vessel networks in vascularized micro-organs (Figure 3): HUVEC-216 (P7, Figure 4A), EPC-AD (P6, Figure 4A), and EPC-

N (P5, Figure 4A). These cells were loaded into the microfluidic devices with and without HCT116 cancer cells. Fluorescent images of the endothelial vessel networks were captured until day 6 post-loading. Imaging-based vessel development quantification was performed (Figures 4A–C, right panels). Time trends in development vascular networks shows that while the rate of the network development was largely indistinguishable between micro-organs and micro-tumors with HUVEC-216 cells, total length of the networks increased significantly faster in micro-tumors with EPC-AD and EPC-N cells. On day 6, where mature vessel networks were established in devices with every EC type, they were characterized for additional parameters of total vessel length, average vessel length, vessel area, and total number of junctions (Figure 4D). Similar to the experiments shown in Figure 2, the architecture and permeability of vascularized micro-organ or micro-tumor networks seeded with the same type of the EC were independent of the presence of HCT116 tumor cells. Similarly, minor non-significant differences in the vascular network parameters were found in micro-organs seeded with different EC lines. However, for total and average vessel length phenotype, the differences between EC sources were more pronounced and significant depending on the cell source. These results suggest that the development and lumenization of endothelial microvascular vessel network are not only cell line-dependent and age-related, but also depend on the cell source - HUVEC cells tend to develop more robust vessel networks, especially in the presence of tumor cells.

3.3. Use of the vascularized micro-tumor model for drug safety testing.

A vascularized tumor model based on the microfluidic platform that can deliver a drug to the tumor in a platform that is mimicking *in vivo* tissue architecture is attractive for application in anti-cancer drug screening (Hachey and Hughes 2018; Phan et al. 2017; Sobrino et al. 2016). Screening assays require reasonable throughput and the complexity of the MPS is a common impediment for their use in early stage drug development. Still, the ability to monitor tumor-vasculature interactions and distinguish between effects on the EC and those on tumor cells are major advantages of the MPS. Here, we selected two drugs, Vincristine and Sorafenib, that were previously tested as part of a blinded primary drug screening of ten FDA-approved anti-cancer compounds at 1 μM concentration (Phan et al. 2017). In that study, Vincristine was identified as active on EC (total vessel length) and marginally active on HCT116 cells (cell death); Sorafenib was without effect in both phenotypes. To demonstrate the potential use of this MPS in another laboratory for anti-cancer drug screening in a time- and concentration-response design, HCT116 tumor cells were embedded with EPC-AD endothelial and NHFL cells to create a vascularized micro-tumor model for drug screening. The VMTs were allowed to develop for 7 days prior to drug exposure. On day 6 post-loading, after the establishment of a perfusable endothelial microvascular vessel network was confirmed (data not shown), drugs were introduced into devices at different concentrations through medium reservoir and channels. After 48 hr exposure, treatment medium was replaced with fresh EGM-2, then the culture was continued for additional 48 hrs.

Figure 5 shows the results of a drug screening study for Vincristine (1–1,000 nM) and Sorafenib (0.1–100 μM) before drug addition (0 hr), after 48 hrs of drug treatment (48 hr), and 48 hours after drug withdrawal (96 hr). The microscopic images of the vascular

networks and tumor foci show that while in vehicle-treated devices the tumor foci growth progresses, in both Vincristine [1,000 nm] (Figure 5B) and Sorafenib [100 μM] (Figure 5C) -treated devices the tumor foci growth is stunted overall, and some of the foci are regressing. At the same time, it is also obvious that the vascular network is also negatively impacted by both drugs at these top concentrations tested, and that the effect is also time-dependent. A detailed time-course of the effects on HCT116 and EC is shown in Figures 5D–F. Effects of Vincristine (Figure 5D) on tumor cell growth were linear with time and dose-dependent; however, the effects on EC networks were more complex – at two lower doses (1–10 nM) the cell recover after the drug is removed, but the networks are permanently damaged at concentrations at 100 nM and above. A concentration-response analysis of these effects at 96 hr showed that HCT116 cells (IC_{50}=1.1 nM) were about 50-fold more sensitive to vincristine than were EC (IC_{50}=64 nM). Interestingly, when the HCT116 and EPC-AD cells were cultured separately in traditional monolayer 2D culture, Vincristine showed nearly identical potency on each cell type.

In experiments with Sorafenib (Figure 5E), time- and concentration-dependent effects were observed only at concentrations at 30 μM or above for HCT116 cells and at 100 μM for EC. While the difference between Sorafenib potency in its effects on cancer vs EC was only 4-fold (IC_{50}=21 vs 87 μM, respectively), there was a dramatic difference in effects between vascularized micro-tumors and 2D cultures. The latter failed to distinguish between effects on each cell type as Sorafenib IC_{50S} were about 2 μM for either one. Overall, these drug screening studies in an independent laboratory are important for several reasons. First, they qualitatively replicated the findings of the initial screen conducted by the developer lab in this novel MPS with a different batch of EC (Phan et al. 2017) – we found that Vincristine was active, while Sorafenib was inactive at 1 μM concentration. Second, we show the feasibility of using this complex MPS for time- and dose-response studies. Third, we show that vascularized micro-tumor MPS allow for quantitative differentiation of the cytotoxic effects between cell types and that these results are more informative than studies in 2D cell culture. Even though for Vincristine we found comparable potency effects in MPS and in 2D cultures, clear recovery of the vascular networks was observed in MPS at concentrations that were cytotoxic in 2D EC cultures. The results for Sorafenib are even more striking as there was not only a 10-fold or more difference with respect to potency between MPS and 2D, but also there was no difference in effects on HCT116 and EC when tested in 2D. This result is important for drug safety evaluation as it demonstrates more realistic “tissue” concentrations that need to be achieved *in vivo* and that there is still a safety margin, albeit quite narrow, between the effects on tumor cells and EC.

An important additional question related to reproducibility of the findings in this MPS is whether drug potency varies between batches of the EC. To address this important practical question, we seeded vascularized micro-tumors with either EPC-AD or HUVEC-216 cells and conducted a time- and dose-response study with 5-FU (1–1,000 μM) using the protocol identical to that detailed above for Vincristine and Sorafenib. Even though the tumor foci differ between devices (Figures 6A–B), HCT116 cells grew unabated in vehicle-treated vascularized micro-tumors containing either EC type. To the contrary, 5-FU (1,000 μM) suppressed the size of tumor foci in both models, tumor size continued to shrink even after withdrawal of 5-FU. Adverse effects on the vascular networks were far less pronounced than

those with Vincristine or Sorafenib at the highest concentration (Figures 5 A–C). Quantitative analysis of tumor area in both conditions (Figures 6C–D) showed highly concordant response, both in terms or time- and concentration-effects. The potency of 5-FU against both HCT116 and EC, was remarkably similar, within 10% of each other. HCT116 cells were about 5-fold more sensitive than either EC line. 5-FU had no effect on either EC type in 2D culture, while the potency against HCT116 cells was about 7-fold higher than in the MPS, again showing that the vascularized micro-tumors can be used reproducibly with different EC lines, as long as those cells are known to establish a perfusable network in this MPS.

3.4. Advantages of a perfusable vascular network for drug safety testing.

Lastly, we conducted experiments with EC that did not form a perfusable vascular network and asked a question whether the luminized network affords any benefits for drug screening. The cell matrix in the devices does allow diffusion of small molecules, and even large molecular weight FITC-Dextran would penetrate into the matrix over time from the side perfusion channels (see Figure 3). Thus, even in non-luminized devices drugs would eventually diffuse into the chambers and can interact with both HCT116 and EC.

For these experiments, we used the HUVEC-155 EC line (Figure 7). As observed in previous experiments (Figure 3), these cells established robust EC networks in vascularized micro-tumors; however, they failed to develop a lumen because we observed that FITC-Dextran diffused into the matrix independent of the vascular microtubules (Figure 7A). To demonstrate the advantage of the perfusion in this device, we used vincristine and 5-FU as test compounds and conducted the experiments exactly as detailed in section 3.3. Figure 7B shows that in cells that do not form a luminized network, Vincristine was without effect on growth of HCT116 cells, but had a profound impact on the EC at 1000 nM. Interestingly, 5-FU had some inhibitory effect on HCT116 cell growth, but had no effect on the EC. Quantitative analysis of the time and concentration-dependent effects (Figure 7C) showed that Vincristine did not reach 50% growth inhibition in HCT116 cells, the IC_{50} for endothelial network total vessel length was 47 nM. When compared to the effects in vascularized micro-tumors with perfusable EC tubules (Figure 5), there is a clear difference in potency – no IC_{50} effect when there is no perfusable vessels, as opposed to IC_{50}=1.1 nM when these is media flow through the tissue. The potency against EC tubulogenesis was comparable with or without flow. Results for 5-FU were comparable in terms of the need for a perfused network (Figure 7D). The potency of 5-FU against HCT116 cells in the non-perfusable devices was about 1/3 of that in the perfusable devices seeded with two different EC types. The lower potency in the absence of flow suggests that insufficient drug is reaching the tumor through diffusion alone. As 5-FU is relatively unstable (Murphy et al. 1987) in plasma (50% loss over 24 hours at room temperature, and probably even greater at 37 °C) it is likely that much of the drug is degraded by the time it diffuses to the tumor. 5-FU had no effect on the EC networks in non-perfusable devices, while it had only marginal effect (IC_{50}=249–295 mM) in perfusable vascularized micro-tumors (Figure 6). Maintenance of the vasculature does require some EC proliferation and so the small effect of 5-FU on the perfused vasculature likely reflects this. These results clearly underscore the need for perfusable vessels for unimpeded drug delivery to the tumor cells to achieve

maximum potency. In addition, when vascular networks are perfusable, effects of drugs not only on the tumor cells, but also on the vasculature, can be effectively examined. Specifically, our experiments confirmed that vincristine is a vascular disrupter but 5-FU has no effects on the vascular networks.

4. Conclusions

Microphysiological models represent a major advance for both drug safety and efficacy studies. One area of biomedical research that will benefit from more human-relevant models is vascular biology. Angiostatic and angiogenic drugs are of great interest for the treatment of a variety of pathologic conditions where vascular development is critical for either disease progression (e.g., cancer), or tissue recovery (e.g., ischemic cardiovascular disease); however, reproducible formation of perfusable vascular networks *in vitro* has been a challenge. The recent development of tissue chip-based models for perfusable micro-organs and micro-tumors offers promise of a more physiological model for drug development; however, the technology transfer of complex tissue chips to the end-users is a well-recognized impediment for their broad adoption. In this study, we showed that a human vascularized micro-organ/-tumor model, while complex, is both robust and reproducible when used with appropriately validated EC sources. We describe the steps needed for successful technology transfer of these models between laboratories, and confirm the advantages of this microphysiological system as compared to monolayer cultures or non-perfusable 3D vascular constructs with respect to the effects of anticancer drugs on both endothelial and tumor cells. At the same time, it should be noted that this study does not represent an attempt at formal qualification of these tissue chip models for use in regulatory decision-making. Biological model's qualification requires specification of the context of use by the potential end-users of the model (Marx et al. 2020), as well as testing of a greater number of compounds that will identify performance boundaries that would adequately justify the use of the tool (US FDA 2017).

Supplementary Material

Refer to Web version on PubMed Central for supplementary material.

Acknowledgements:

This work was supported, in part, by grants from the National Institutes of Health [U24 TR001950 and UH3 TR000487]. C.S. was supported, in part, by T32 ES026568. C.C.W.H. also received support from the University of California Irvine Chao Family Comprehensive Cancer Center (CFCCC, P30 CA062203).

References

Atchison L, Zhang H, Cao K and Truskey GA (2017) A Tissue Engineered Blood Vessel Model of Hutchinson-Gilford Progeria Syndrome Using Human iPSC-derived Smooth Muscle Cells. Sci Rep 7, 8168. [PubMed: 28811655]

Barillari G (2020) The Anti-Angiogenic Effects of Anti-Human Immunodeficiency Virus Drugs. Front Oncol 10, 806. [PubMed: 32528888]

Carmeliet P and Jain RK (2011) Molecular mechanisms and clinical applications of angiogenesis. Nature 473, 298–307. [PubMed: 21593862]

Celermajer DS, Sorensen KE, Spiegelhalter DJ, Georgakopoulos D, Robinson J and Deanfield JE (1994) Aging is associated with endothelial dysfunction in healthy men years before the age-related decline in women. J Am Coll Cardiol 24, 471–476. [PubMed: 8034885]

Craige SM, Chen K, Pei Y, Li C, Huang X, Chen C, Shibata R, Sato K, Walsh K and Keaney JF Jr. (2011) NADPH oxidase 4 promotes endothelial angiogenesis through endothelial nitric oxide synthase activation. Circulation 124, 731–740. [PubMed: 21788590]

Dewberry RM, Crossman DC and Francis SE (2003) Interleukin-1 receptor antagonist (IL-1RN) genotype modulates the replicative capacity of human endothelial cells. Circ Res 92, 1285–1287. [PubMed: 12764021]

Erusalimsky JD (2009) Vascular endothelial senescence: from mechanisms to pathophysiology. J Appl Physiol (1985) 106, 326–332. [PubMed: 19036896]

Ewart L, Fabre K, Chakilam A, Dragan Y, Duignan DB, Eswaraka J, Gan J, Guzzie-Peck P, Otieno M, Jeong CG, Keller DA, de Morais SM, Phillips JA, Proctor W, Sura R, Van Vleet T, Watson D, Will Y, Tagle D and Berridge B (2017) Navigating tissue chips from development to dissemination: A pharmaceutical industry perspective. Exp Biol Med (Maywood) 242, 1579–1585. [PubMed: 28622731]

Gebala V, Collins R, Geudens I, Phng LK and Gerhardt H (2016) Blood flow drives lumen formation by inverse membrane blebbing during angiogenesis in vivo. Nat Cell Biol 18, 443–450. [PubMed: 26928868]

Grimm FA, Klaren WD, Li X, Lehmler HJ, Karmakar M, Robertson LW, Chiu WA and Rusyn I (2020) Cardiovascular Effects of Polychlorinated Biphenyls and Their Major Metabolites. Environ Health Perspect 128, 77008. [PubMed: 32701041]

Hachey SJ and Hughes CCW (2018) Applications of tumor chip technology. Lab Chip 18, 2893–2912. [PubMed: 30156248]

Hachey SJ, Movsesyan S, Nguyen QH, Burton-Sojo G, Tankanzyan A, Wu J, Hoang T, Hatch MM, Zhao D, Celaya E, Gomez S, Chen GT, Davis RT, Nee K, Pervolarakis N, Lawson DA, Kessenbrock K, Lee AP, Waterman ML and Hughes CCW (2020) An In Vitro Vascularized Micro-Tumor Model of Human Colorectal Cancer Recapitulates In Vivo Drug Responses. bioRxiv, 2020.2003.2003.973891.

Hadzijusufovic E, Albrecht-Schgoer K, Huber K, Hoermann G, Grebien F, Eisenwort G, Schgoer W, Herndlhofer S, Kaun C, Theurl M, Sperr WR, Rix U, Sadovnik I, Jilma B, Schernthaner GH, Wojta J, Wolf D, Superti-Furga G, Kirchmair R and Valent P (2017) Nilotinib-induced vasculopathy: identification of vascular endothelial cells as a primary target site. Leukemia 31, 2388–2397. [PubMed: 28757617]

Iruela-Arispe ML and Davis GE (2009) Cellular and molecular mechanisms of vascular lumen formation. Dev Cell 16, 222–231. [PubMed: 19217424]

Iwata Y, Klaren WD, Lebakken CS, Grimm FA and Rusyn I (2017) High-Content Assay Multiplexing for Vascular Toxicity Screening in Induced Pluripotent Stem Cell-Derived Endothelial Cells and Human Umbilical Vein Endothelial Cells. Assay Drug Dev Technol 15, 267–279. [PubMed: 28771372]

Jain RK, Safabakhsh N, Sckell A, Chen Y, Jiang P, Benjamin L, Yuan F and Keshet E (1998) Endothelial cell death, angiogenesis, and microvascular function after castration in an androgen-dependent tumor: role of vascular endothelial growth factor. Proc Natl Acad Sci U S A 95, 10820–10825. [PubMed: 9724788]

Jeon JS, Bersini S, Gilardi M, Dubini G, Charest JL, Moretti M and Kamm RD (2015) Human 3D vascularized organotypic microfluidic assays to study breast cancer cell extravasation. Proc Natl Acad Sci U S A 112, 214–219. [PubMed: 25524628]

Jeon JS, Bersini S, Whisler JA, Chen MB, Dubini G, Charest JL, Moretti M and Kamm RD (2014) Generation of 3D functional microvascular networks with human mesenchymal stem cells in microfluidic systems. Integr Biol (Camb) 6, 555–563. [PubMed: 24676392]

Kaur J, Adya R, Tan BK, Chen J and Randeva HS (2010) Identification of chemerin receptor (ChemR23) in human endothelial cells: chemerin-induced endothelial angiogenesis. Biochem Biophys Res Commun 391, 1762–1768. [PubMed: 20044979]

Lacal PM and Graziani G (2018) Therapeutic implication of vascular endothelial growth factor receptor-1 (VEGFR-1) targeting in cancer cells and tumor microenvironment by competitive and non-competitive inhibitors. Pharmacol Res 136, 97–107. [PubMed: 30170190]

Lamalice L, Le Boeuf F and Huot J (2007) Endothelial cell migration during angiogenesis. Circ Res 100, 782–794. [PubMed: 17395884]

Lawal AO, Davids LM and Marnewick JL (2016) Diesel exhaust particles and endothelial cells dysfunction: An update. Toxicol In Vitro 32, 92–104. [PubMed: 26721178]

Livingston CA, Fabre KM and Tagle DA (2016) Facilitating the commercialization and use of organ platforms generated by the microphysiological systems (Tissue Chip) program through public-private partnerships. Comput Struct Biotechnol J 14, 207–210. [PubMed: 27904714]

Maass C, Sorensen NB, Himmelfarb J, Kelly EJ, Stokes CL and Cirit M (2019) Translational Assessment of Drug-Induced Proximal Tubule Injury Using a Kidney Microphysiological System. CPT Pharmacometrics Syst Pharmacol 8, 316–325. [PubMed: 30869201]

Marx U, Akabane T, Andersson TB, Baker E, Beilmann M, Beken S, Brendler-Schwaab S, Cirit M, David R, Dehne EM, Durieux I, Ewart L, Fitzpatrick SC, Frey O, Fuchs F, Griffith LG, Hamilton GA, Hartung T, Hoeng J, Hogberg H, Hughes DJ, Ingber DE, Iskandar A, Kanamori T, Kojima H, Kuehnl J, Leist M, Li B, Loskill P, Mendrick DL, Neumann T, Pallocca G, Rusyn I, Smirnova L, Steger-Hartmann T, Tagle DA, Tonevitsky A, Tsyb S, Trapecar M, Van de Water B, Van den Eijnden-van Raaij J, Vulto P, Watanabe K, Wolf A, Zhou X and Roth A (2020) Biology-inspired microphysiological systems to advance patient benefit and animal welfare in drug development. ALTEX 37, 365–394. [PubMed: 32113184]

Moya ML, Hsu YH, Lee AP, Hughes CC and George SC (2013) In vitro perfused human capillary networks. Tissue Eng Part C Methods 19, 730–737. [PubMed: 23320912]

Murphy RF, Balis FM and Poplack DG (1987) Stability of 5-fluorouracil in whole blood and plasma. Clin Chem 33, 2299–2300. [PubMed: 3484334]

Nakatsu MN, Sainson RC, Aoto JN, Taylor KL, Aitkenhead M, Perez-del-Pulgar S, Carpenter PM and Hughes CC (2003) Angiogenic sprouting and capillary lumen formation modeled by human umbilical vein endothelial cells (HUVEC) in fibrin gels: the role of fibroblasts and Angiopoietin-1. Microvasc Res 66, 102–112. [PubMed: 12935768]

Nguyen DH, Stapleton SC, Yang MT, Cha SS, Choi CK, Galie PA and Chen CS (2013) Biomimetic model to reconstitute angiogenic sprouting morphogenesis in vitro. Proc Natl Acad Sci U S A 110, 6712–6717. [PubMed: 23569284]

Nguyen EH, Daly WT, Le NNT, Farnoodian M, Belair DG, Schwartz MP, Lebakken CS, Ananiev GE, Saghiri MA, Knudsen TB, Sheibani N and Murphy WL (2017) Versatile synthetic alternatives to Matrigel for vascular toxicity screening and stem cell expansion. Nat Biomed Eng 1.

Norton KA and Popel AS (2016) Effects of endothelial cell proliferation and migration rates in a computational model of sprouting angiogenesis. Sci Rep 6, 36992. [PubMed: 27841344]

Nowak-Sliwinska P, Alitalo K, Allen E, Anisimov A, Aplin AC, Auerbach R, Augustin HG, Bates DO, van Beijnum JR, Bender RHF, Bergers G, Bikfalvi A, Bischoff J, Bock BC, Brooks PC, Bussolino F, Cakir B, Carmeliet P, Castranova D, Cimpean AM, Cleaver O, Coukos G, Davis GE, De Palma M, Dimberg A, Dings RPM, Djonov V, Dudley AC, Dufton NP, Fendt SM, Ferrara N, Fruttiger M, Fukumura D, Ghesquiere B, Gong Y, Griffin RJ, Harris AL, Hughes CCW, Hultgren NW, Iruela-Arispe ML, Irving M, Jain RK, Kalluri R, Kalucka J, Kerbel RS, Kitajewski J, Klaassen I, Kleinmann HK, Koolwijk P, Kuczynski E, Kwak BR, Marien K, Melero-Martin JM, Munn LL, Nicosia RF, Noel A, Nurro J, Olsson AK, Petrova TV, Pietras K, Pili R, Pollard JW, Post MJ, Quax PHA, Rabinovich GA, Raica M, Randi AM, Ribatti D, Ruegg C, Schlingemann RO, Schulte-Merker S, Smith LEH, Song JW, Stacker SA, Stalin J, Stratman AN, Van de Velde M, van Hinsbergh VWM, Vermeulen PB, Waltenberger J, Weinstein BM, Xin H, Yetkin-Arik B, Yla-Herttuala S, Yoder MC and Griffioen AW (2018) Consensus guidelines for the use and interpretation of angiogenesis assays. Angiogenesis 21, 425–532. [PubMed: 29766399]

Peng Z, Shu B, Zhang Y and Wang M (2019) Endothelial Response to Pathophysiological Stress. Arterioscler Thromb Vasc Biol 39, e233–e243. [PubMed: 31644356]

Phan DTT, Wang X, Craver BM, Sobrino A, Zhao D, Chen JC, Lee LYN, George SC, Lee AP and Hughes CCW (2017) A vascularized and perfused organ-on-a-chip platform for large-scale drug screening applications. Lab Chip 17, 511–520. [PubMed: 28092382]

Pinheiro EA, Magdy T and Burridge PW (2020) Human In Vitro Models for Assessing the Genomic Basis of Chemotherapy-Induced Cardiovascular Toxicity. J Cardiovasc Transl Res.

Rivard A, Fabre JE, Silver M, Chen D, Murohara T, Kearney M, Magner M, Asahara T and Isner JM (1999) Age-dependent impairment of angiogenesis. Circulation 99, 111–120. [PubMed: 9884387]

Ross S, Gerstein H and Pare G (2018) The Genetic Link Between Diabetes and Atherosclerosis. Can J Cardiol 34, 565–574. [PubMed: 29731020]

Sakolish C, House JS, Chramiec A, Liu Y, Chen Z, Halligan SP, Vunjak-Novakovic G and Rusyn I (2020) Tissue-Engineered Bone Tumor as a Reproducible Human in Vitro Model for Studies of Anticancer Drugs. Toxicol Sci 173, 65–76. [PubMed: 31626302]

Sakolish C, Weber EJ, Kelly EJ, Himmelfarb J, Mouneimne R, Grimm FA, House JS, Wade T, Han A, Chiu WA and Rusyn I (2018) Technology Transfer of the Microphysiological Systems: A Case Study of the Human Proximal Tubule Tissue Chip. Sci Rep 8, 14882. [PubMed: 30291268]

Schurdak M, Vernetti L, Bergenthal L, Wolter QK, Shun TY, Karcher S, Taylor DL and Gough A (2020) Applications of the microphysiology systems database for experimental ADME-Tox and disease models. Lab Chip 20, 1472–1492. [PubMed: 32211684]

Semeraro F, Morescalchi F, Duse S, Gambicorti E, Cancarini A and Costagliola C (2015) Pharmacokinetic and Pharmacodynamic Properties of Anti-VEGF Drugs After Intravitreal Injection. Curr Drug Metab 16, 572–584. [PubMed: 26424177]

Sobrino A, Phan DT, Datta R, Wang X, Hachey SJ, Romero-Lopez M, Gratton E, Lee AP, George SC and Hughes CC (2016) 3D microtumors in vitro supported by perfused vascular networks. Sci Rep 6, 31589. [PubMed: 27549930]

US FDA. (2017) FDA'S Predictive Toxicology Roadmap. U.S. Food and Drug Administration, Silver Spring, MD.

van der Loo B, Labugger R, Skepper JN, Bachschmid M, Kilo J, Powell JM, Palacios-Callender M, Erusalimsky JD, Quaschning T, Malinski T, Gygi D, Ullrich V and Luscher TF (2000) Enhanced peroxynitrite formation is associated with vascular aging. J Exp Med 192, 1731–1744. [PubMed: 11120770]

Viallard C and Larrivee B (2017) Tumor angiogenesis and vascular normalization: alternative therapeutic targets. Angiogenesis 20, 409–426. [PubMed: 28660302]

Weinsaft JW and Edelberg JM (2001) Aging-associated changes in vascular activity: a potential link to geriatric cardiovascular disease. Am J Geriatr Cardiol 10, 348–354. [PubMed: 11684920]

Yeon JH, Ryu HR, Chung M, Hu QP and Jeon NL (2012) In vitro formation and characterization of a perfusable three-dimensional tubular capillary network in microfluidic devices. Lab Chip 12, 2815–2822. [PubMed: 22767334]

Yu JL, Rak JW, Carmeliet P, Nagy A, Kerbel RS and Coomber BL (2001) Heterogeneous vascular dependence of tumor cell populations. Am J Pathol 158, 1325–1334. [PubMed: 11290550]

Zhang Q, Zhang X and Truskey GA (2020) Vascular Microphysiological Systems to Model Diseases. Cell Gene Ther Insights 6, 93–102. [PubMed: 32431950]

Zito C, Manganaro R, Carerj S, Antonini-Canterin F and Benedetto F (2020) Peripheral Artery Disease and Stroke. J Cardiovasc Echogr 30, S17–S25. [PubMed: 32566462]

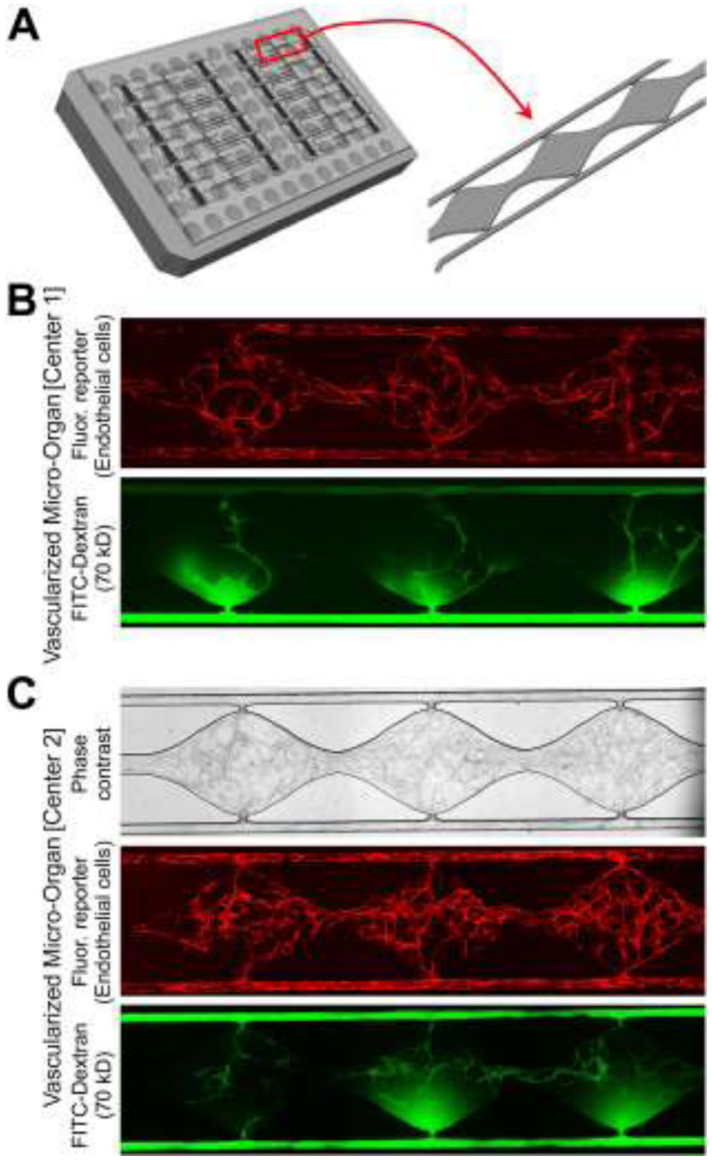

Figure 1. Microfluidic vascularized micro-organ device.

(A) Platform schematic based on the 96-well plate design. The device (Hachey et al. 2020; Phan et al. 2017) consists of a PDMS layer containing the microfluidics, and a transparent polymer membrane that are bonded to a bottomless 96-well plate. The plate contains 12 three-chamber devices that are seeded and perfused as a conjoined unit. Each tissue chamber in a unit is 2×1×0.1 mm. **(B)** Representative micro-photographic images (4×) of a three-chamber unit generated in Laboratory 1 (University of California, Irvine). The unit was seeded with EPC-N (P5) EC and normal human lung fibroblasts (NHLFs) and imaged on day 6 for a fluorescent reporter (mCherry) expressed by EC before, or after (bottom) addition of FITC-Dextran (70 kDa, green fluorescence). **(C)** Representative micro-photographic images (4×) of a three-chamber unit generated in Laboratory 2 (Texas A&M University). The unit was seeded with the same cells as in (B). Top image is a phase-contrast

view, the middle is imaging for the fluorescent reporter (mCherry) expressed by EC before, or after (bottom) addition of FITC-Dextran (70 kDa).

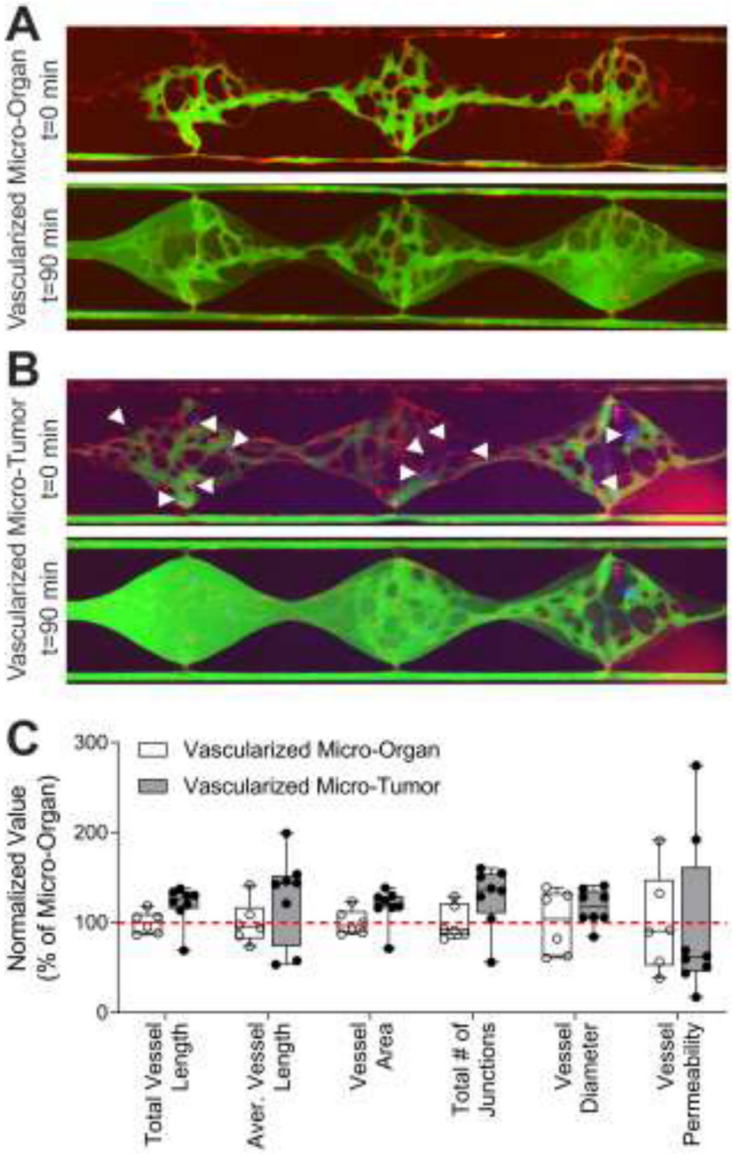

Figure 2.

Establishment of vascularized micro-organs and micro-tumors, and vascular network characterization. **(A)** Vascularized micro-organs were established with EPC-N (P5) EC and NHLFs. A representative micro-photographic image (4×) of a three-chamber unit on day 6 post-seeding. Red fluorescence is mCherry-expressing EC and green fluorescence is FITC-Dextran (70 kDa) added to the vessel network. Images were taken immediately after adding FITC-Dextran (top, t=0 min) or 90 minutes after (bottom). Each tissue chamber is 2×1×0.1 mm. **(B)** Vascularized micro-tumors were established with EPC-N (P5) EC, normal human lung fibroblasts (NHLFs) and HCT116 tumor cells. A representative micro-photographic image (4×) of a three-chamber unit on day 6 post-seeding. Red and green fluorescence are as detailed in panel (B). Blue is HCT116 cells. **(C)** Quantification of the vascular networks in micro-organs (white box-and-whiskers) and micro-tumors (gray box-and-whiskers). Values are mean±SEM (n=6–8) normalized to vascularized micro-organ values. Dotted line

indicates 100% value. Boxes are inter-quartile range, the lines are median values, the whiskers are min and max values. Each replicate is indicated by a black dot.

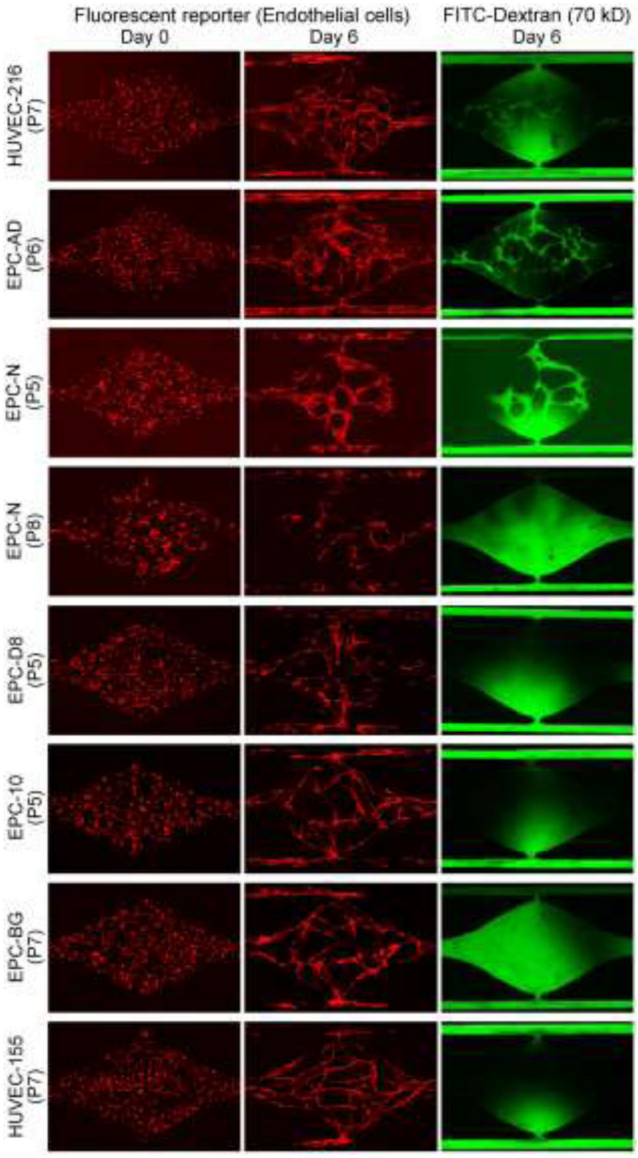

Figure 3. Vascularized micro-organs that have perfusable networks can be established with some, but not all EC lines.

A representative micro-photographic image (4×) of a three-chamber unit on day 0 (left most column) and day 6 (middle and right most columns) post-seeding with 7 different EC lines (cell lines codes and passage numbers are indicated on the graph). Red fluorescence is mCherry-expressing EC and green fluorescence is FITC-Dextran (70 kDa) added to the vessel network. Images were taken 90 min after adding FITC-Dextran. Each tissue chamber is 2×1×0.1 mm.

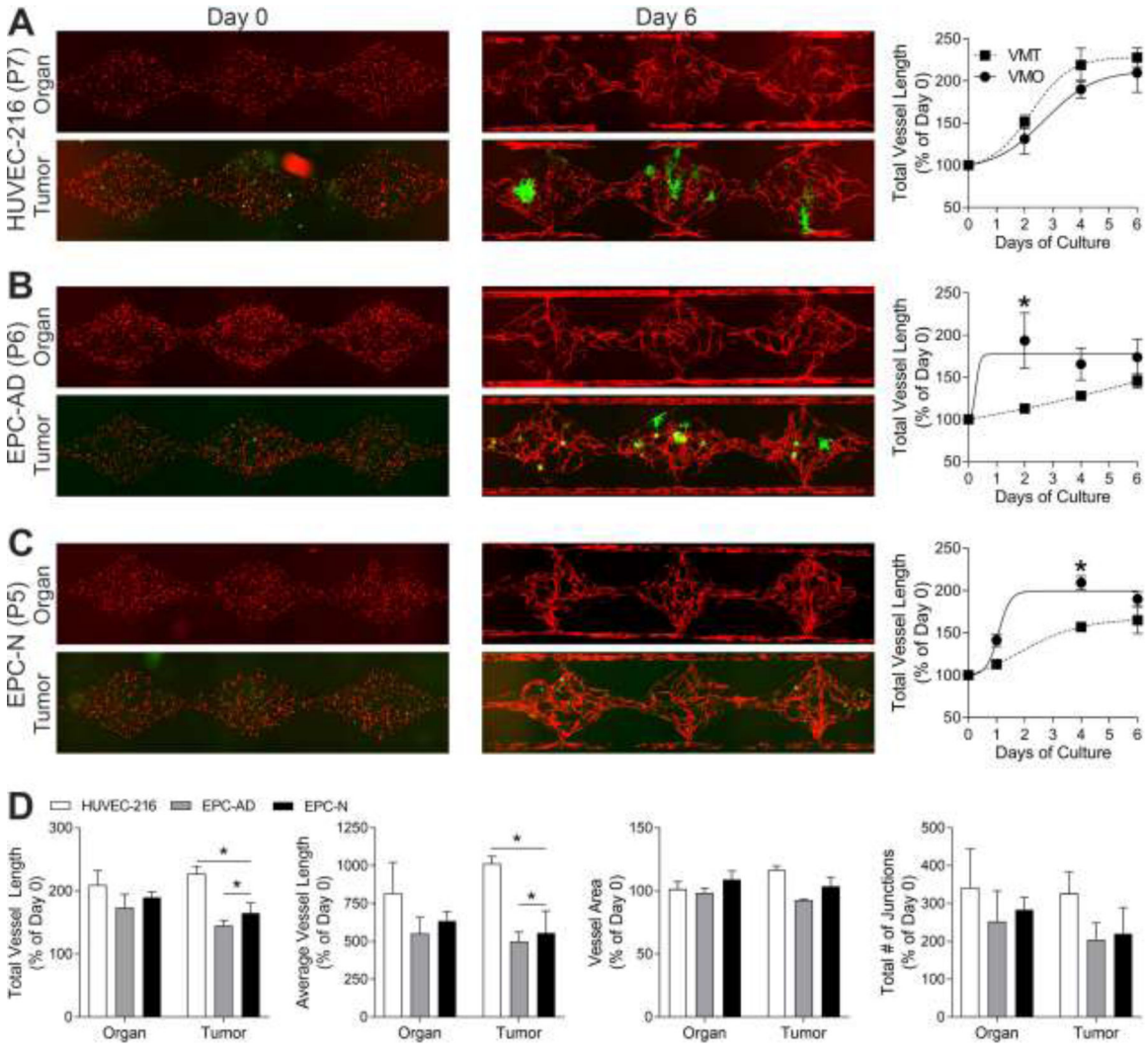

Figure 4. Dynamics of blood vessel formation in vascularized micro-organs or -tumors established with different EC lines.

(A) Example of HUVEC-216 (P7) cell line. A representative micro-photographic image (4×) of a single chamber in a unit on day 0 (left most column) and day 6 (middle column) post-seeding. Red is EC and green is HCT116 cells. Top images are for vascularized micro-organs and bottom for micro-tumor. Each tissue chamber is 2×1×0.1 mm. Right most panel is a graph of the Hill model fits to the data for total vessel length endpoint that were collected over 6 days of culture as indicated in the x-axis. Data were normalized to the values on day 0. Vascularized micro-organ (VMO) data are indicated by black circles and a solid line. Vascularized micro-tumor (VMT) data are indicated by black squares and a dashed line. Data are mean±SEM (n=3–6). **(B)** Example of EPC-AD (P6) cell line. Image and line graph description is same as in (A). Asterisk (*) indicates a significant difference ($p<0.05$) between VMO and VMT on day 2 using two-way ANOVA followed by Sidak's multiple comparisons test. **(C)** Example of EPC-N (P5) cell line. Image and line graph description is same as in (A). Asterisk (*) indicates a significant difference ($p<0.05$) between VMO and VMT on day 4 using two-way ANOVA followed by Sidak's multiple

comparisons test. **(D)** Quantification of the vascular networks in micro-organs and micro-tumors. Each bar corresponds to one of three EC lines as indicated. Values are mean±SEM (n=3–6) normalized to day 0 values. Asterisk (*) indicates a significant difference ($p<0.05$) between cell lines on day 6 using two-way ANOVA followed by Tukey's multiple comparisons test.

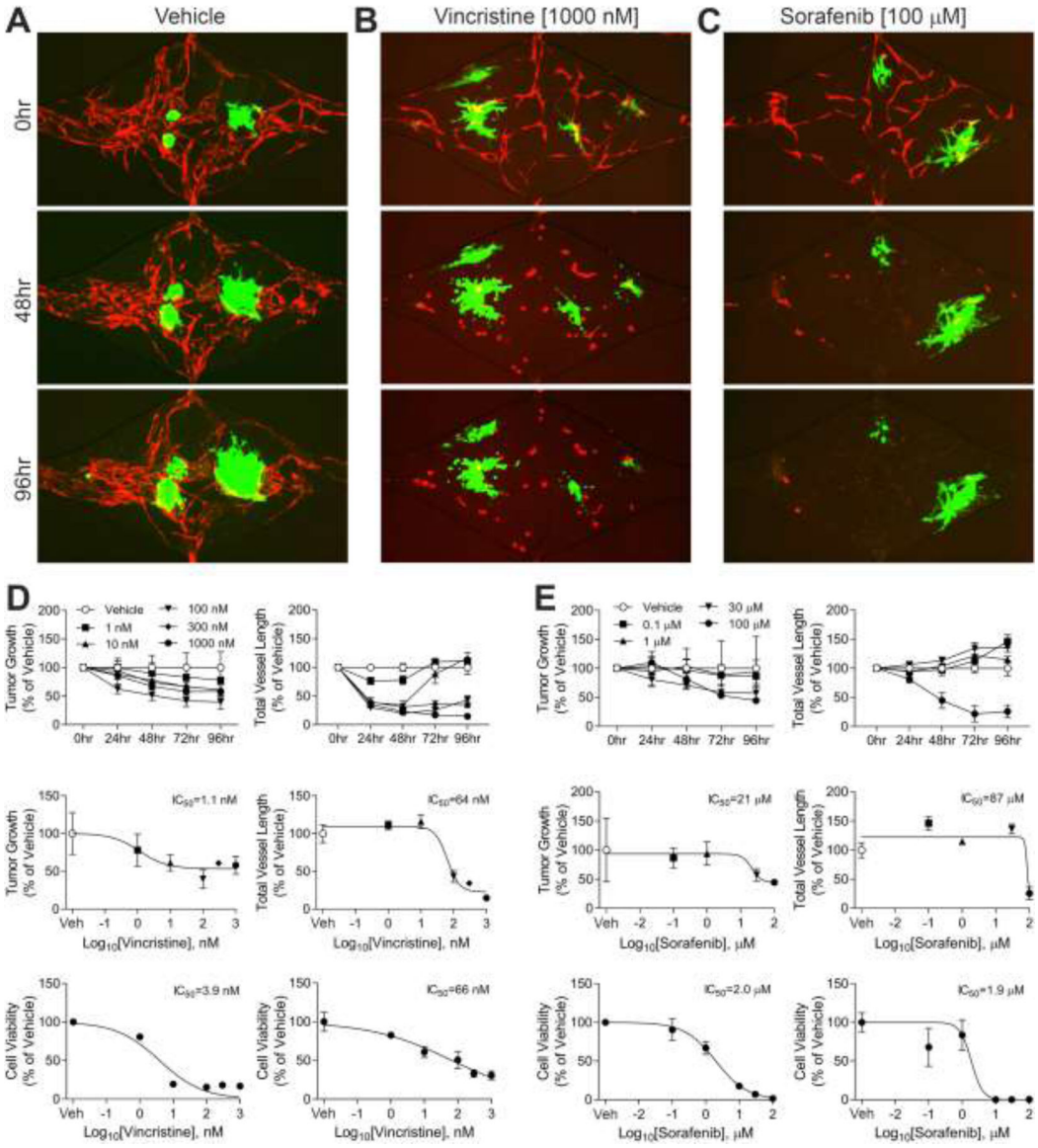

Figure 5. Anticancer drug effects on tumor (HCT116) and endothelial (EPC-AD, P6) cells in the vascularized micro-tumor MPS or 2D culture.

(A) Example of a time-course in vehicle-treated vascularized micro-tumors. A representative micro-photographic image (4×) of a single chamber in a unit on day 6 (top, 0 hr), day 8 (middle, 48 hr), or day 10 (bottom, 96 hr) post-seeding. Hours correspond to the time of treatment with vehicle or drug. Red is EC and green is HCT116 cells. Each tissue chamber is 2×1×0.1 mm. **(B)** Example of a time-course with Vincristine (1,000 nM)-treated vascularized micro-tumors. **(C)** Example of a time-course with Sorafenib (100 μM)-treated vascularized micro-tumors. **(D)** Dose- and time-course effects of Vincristine. Left panels are data for HCT116 cells, right panels are data for EC. Top panels are data from vascularized micro-tumors that include both time- and concentration-response. Middle panels are dose-response at 96 hr time point. Bottom panels are dose-response data from 2D experiments after 96 hrs. Data are mean±SEM (n=3) normalized to vehicle-treated values. Where error

bars are not visible, they are smaller than the symbol. **(E)** Same as (D) but for Sorafenib-treated MPS or cells.

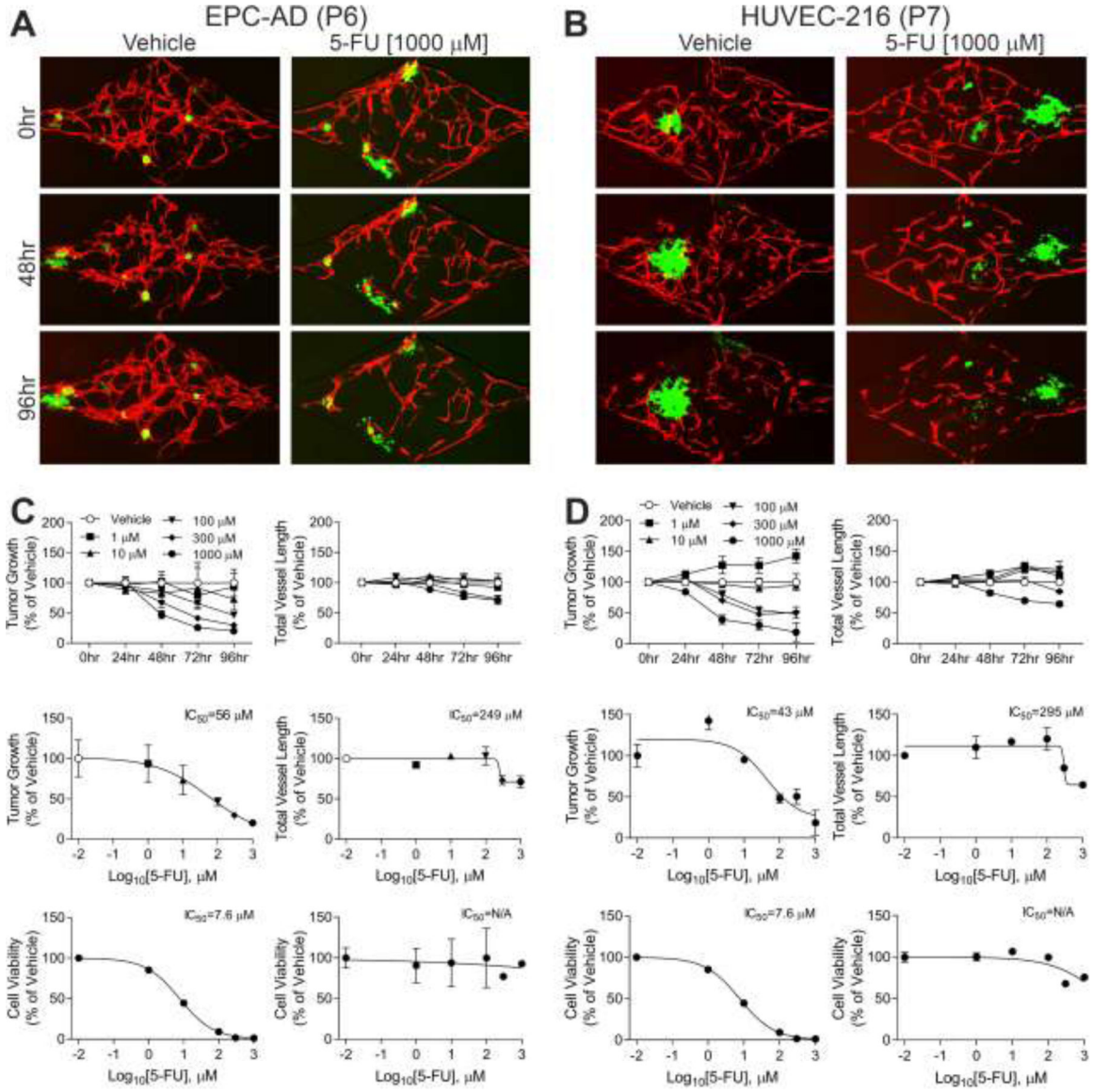

Figure 6. Cell to cell variability is low in anticancer drug effects on tumor (HCT116) and endothelial (EPC-AD, P6 and HUVEC-216, P7) cells lines in the vascularized micro-tumor MPS or 2D culture.

(A) Example of a time-course in vehicle- (left panel) and 5-fluorouracil (FU, 1,000 μM, right panel)-treated vascularized micro-tumors seeded with EPC-AD, P6 EC line. A representative micro-photographic image (4×) of a single chamber in a unit on day 6 (top, 0 hr), day 8 (middle, 48 hr), or day 10 (bottom, 96 hr) post-seeding. Hours correspond to the time of treatment with vehicle or drug. Red is EC and green is HCT116 cells. Each tissue chamber is 2×1×0.1 mm. **(B)** Same as in (A) but for vascularized micro-tumors seeded with HUVEC-216, P7 EC line. **(C)** Dose- and time-course effects of 5-FU in vascularized micro-tumors seeded with EPC-AD, P6 EC line. Left panels are data for HCT116 cells, right panels are data for EC. Top panels are data from vascularized micro-tumors that include both time- and concentration-response. Middle panels are dose-response at 96 hr time point. Bottom panels are dose-response data from 2D experiments after 96 hrs. Data are mean

±SEM (n=3) normalized to vehicle-treated values. Where error bars are not visible, they are smaller than the symbol. **(D)** Same as in (C) but for vascularized micro-tumors seeded with HUVEC-216, P7 EC line. HCT116 data are same as in (C).

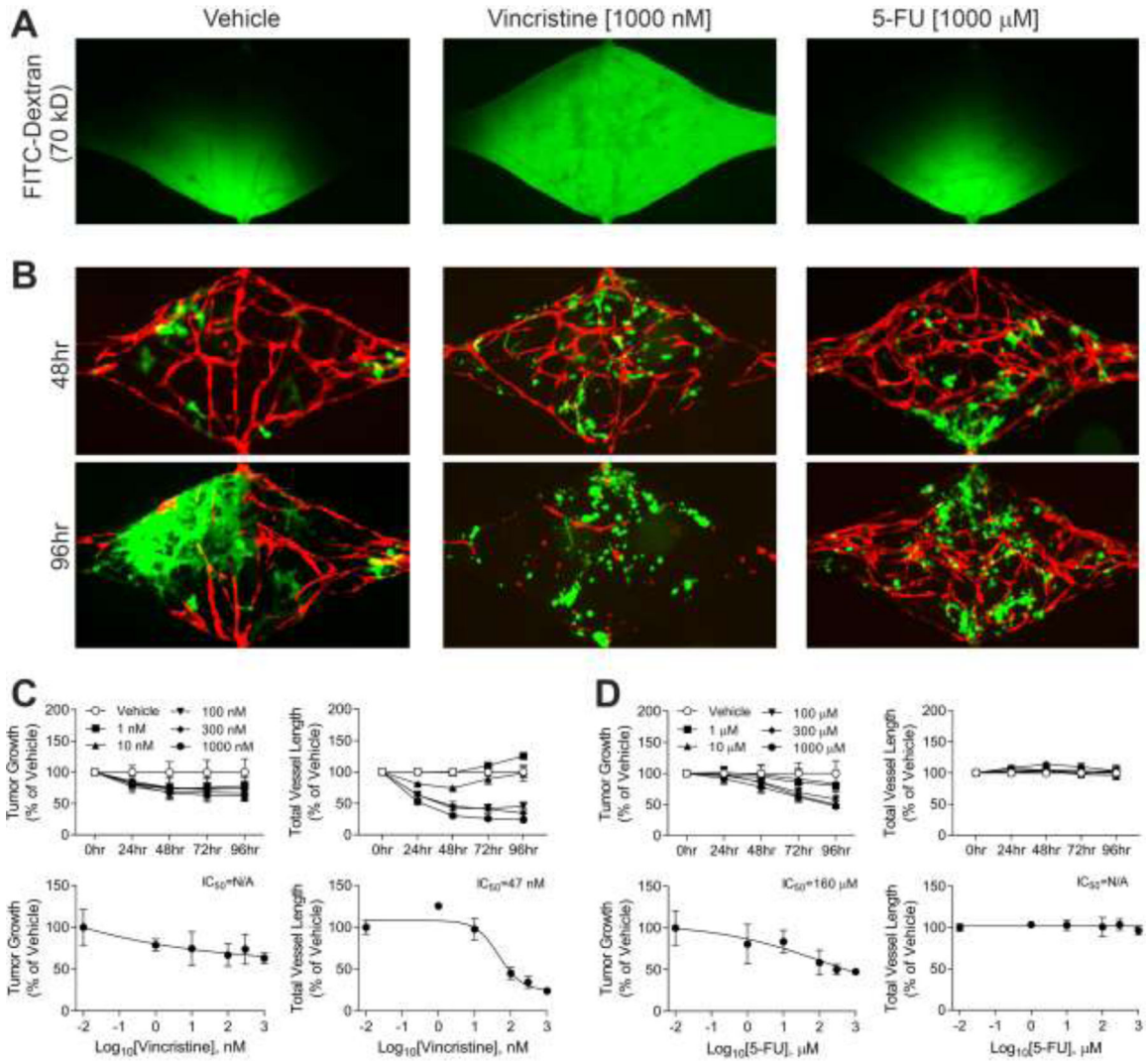

Figure 7. Anticancer drug effects on tumor cells in the vascularized micro-tumor MPS depend on the presence of a perfusable vessel network.

(A) Demonstration that no perfusable network was established by HUVEC-155, P7 cell line treated with vehicle (left panel), Vincristine (1,000 nM, middle panel), or 5-FU (1,000 μM, right panel). Green fluorescence is FITC-Dextran (70 kDa) added to the vessel network. Images were taken 90 min after adding FITC-Dextran. Each tissue chamber is 2×1×0.1 mm. **(B)** Example of a time-course of vehicle or drug effects in vascularized micro-tumors seeded with HUVEC-155, P7 EC line. A representative micro-photographic image (4×) of a single chamber in a unit on day 8 (top, 48 hr), or day 10 (bottom, 96 hr) post-seeding. Hours correspond to the time of treatment with vehicle or drug. Red is EC and green is HCT116 cells. **(C)** Dose- and time-course effects of Vincristine. Left panels are data for HCT116 cells, right panels are data for EC. Top panels are data from vascularized micro-tumors that include both time- and concentration-response. Bottom panels are dose-response at 96 hr time point. Data are mean±SEM (n=3) normalized to vehicle-treated values. Where error bars are not visible, they are smaller than the symbol. **(D)** Same as in (C) but for 5-FU.